Kinetic nucleation model for free expanding water condensation plume simulations

Zheng Li,[1,a)] Jiaqiang Zhong,[1,b)] Deborah A. Levin,[1,c)] and Barbara J. Garrison[2,d)]
[1]*Department of Aerospace Engineering, The Pennsylvania State University, University Park, Pennsylvania 16802, USA*
[2]*Department of Chemistry, The Pennsylvania State University, University Park, Pennsylvania 16802, USA*

(Received 22 January 2009; accepted 15 April 2009; published online 7 May 2009)

Recent direct simulation Monte Carlo (DSMC) simulations of homogeneous condensation in free expansion water plumes [Z. Li, J. Zhong, D. A. Levin, and B. Garrison, AIAA J. **47**, 1241 (2009)] show that the nucleation rate is a key factor for accurately modeling condensation phenomenon. In this work, we use molecular dynamics (MD) simulations of a free expansion to explore the microscopic mechanisms of water dimer formation and develop collision models required by DSMC. Bimolecular and termolecular dimer cluster formation mechanisms are considered and the former is found to be the main mechanism in expanding flows to vacuum. MD simulations between two water molecules using the simple point charge intermolecular potential were performed to predict the bimolecular dimer formation probability and the probability was found to decrease with collision energy. The formation probabilities and postcollisional velocity and energy distributions were then integrated into DSMC simulations of a free expansion of an orifice condensation plume with different chamber stagnation temperatures and pressures. The dimer mole fraction was found to increase with distance from the orifice and become constant after a distance of about two orifice diameters. Similar to experiment, the terminal dimer mole fraction was found to decrease with chamber stagnation temperatures and increase linearly with chamber stagnation pressures which is consistent with a bimolecular nucleation mechanism. © *2009 American Institute of Physics*.
[DOI: 10.1063/1.3129804]

I. INTRODUCTION

The study of condensation phenomenon observed in free expansion plumes during the past several decades has a number of important aerospace applications. When a gas expands from spacecraft thruster nozzles to the space near-vacuum environment, its speed increases and its temperature decreases, and the flow becomes supersaturated. The condensed clusters formed by homogeneous condensation are a precursor process that can contribute to various operational problems. For example, spaceborne optical systems may be sensitive to optical contamination of their local environment by gases or condensate particles produced by the operation of attitude control system (ACS) jets. In addition, the operation of solar cell arrays and the heat rejection capabilities of thermal protection materials may also be degraded. To improve modeling of homogeneous condensation for realistic space propellants, comparisons can be made with remote observations of space plume condensation phenomena or small jet laboratory measurements. With respect to space observations of condensation, strong visible and UV signals due to solar scattering from condensed ACS jet exhaust gases have been observed and analyzed and condensed argon clusters from the propellant are thought to be responsible for this phenomenon.[1] In the 1995–1996 time frame, the Astra-2 experiment flew a small cold argon thruster to study far-field plume phenomenology. The flow inside the nozzle, near vicinity, and far field of the plume was numerically studied by Ivanov and Markelov.[2] A comparison of numerical predictions and experimental data of the angular distribution of the relative pressure in the far field of the plume showed that it is necessary to take into account the process of argon condensation both inside the nozzle and in the near vicinity. A spectacular visible plume of the translunar injection burn of a Saturn IV B spacecraft during the Apollo 8 mission was photographed by the Smithsonian Astrophysical Observatory on Mt. Haleakela, Hawaii. Analysis of visible signals indicated that condensed exhaust plume water vapor was able to produce large solar scattering signals.[3]

Laboratory measurements, in contrast to space observations, provide a better source of data to validate the gas dynamics of a condensating supersonic expansion. We mention here only a few of the important laboratory data sets. Hagena and Obert[4] performed a series of expanding plume experiments on homogeneous condensation for different gases and measured cluster beams from the core of the plume flow field. From these measurements, he deduced a scaling law that suggested that specific combinations of source pressure, temperature, and nozzle geometry will result in cluster beams with the same mean cluster size. An Arnold Engineering Development Center program known as CONSET (Ref. 5) performed experiments to determine the onset and growth

[a)]Electronic mail: zul107@psu.edu.
[b)]Electronic mail: jxz194@psu.edu.
[c)]Electronic mail: dalevin@psu.edu.
[d)]Electronic mail: bjg@psu.edu.

properties of condensate clusters in a typical exhaust plume flow field and the dependence of the condensation process on nozzle geometry, reservoir conditions, molecular parameters, and flow species, such as argon, oxygen, and water. Laser-Rayleigh scattering was used to characterize the distribution and growth of clusters as well as to determine the condensation onset and scaling law experiments were performed for different species including argon, nitrogen, water, and carbon dioxide. Koppenwallner and Dankert[6] also studied condensation in free jet expansions from sonic orifices for different stagnation temperatures, pressures, and nozzle throat diameters with nitrogen, water vapor, and argon as test gases. Both pressure probe and laser light scattering were used to detect the condensation onset points on the centerline of all free jets and the results were compared to classical nucleation theory (CNT) theory. More recently, laser-Rayleigh scattering measurements have been combined with Raman spectroscopy to provide axial as well as radial cluster size and number density for a carbon dioxide free jet expansion.[7]

The modeling of condensing plumes requires a versatile gas dynamic approach that can simulate multiple flow regimes as well as utilize molecular dynamics based collision models. The freely expanding flow is characterized by a large variation in number density from the nozzle exit to the plume far field. The Knudsen number, defined as the ratio of mean free path to the characteristic length (the nozzle exit diameter), is typically on the order of 10^{-3} at the exit, a value where Navier–Stokes equation is applicable. However, as the gas expands, the Knudsen number increases quickly to a region where the continuum flow assumption is no longer valid and transitional flow effects must be considered. In this work, we use the direct simulation Monte Carlo (DSMC) method for the high Knudsen number regions. DSMC (Ref. 8) is a numerical method for modeling transitional to rarefied gas flows, in which the mean free path of a molecule is of the same order (or greater) than a representative physical length scale (i.e., the Knudsen number Kn is greater than 1). The DSMC method models flows using computational particles that represent a large number of real molecules in a probabilistic simulation to solve the Boltzmann equation. Particles are moved through a simulation of physical space in a manner that is directly coupled to the local mean time between collisions such that flow characteristics can be modeled. Interparticle collisions and particle-surface collisions are calculated using probabilistic, phenomenological models. Common collision models include the hard sphere (HS) model, the variable HS (VHS) model, and the variable soft sphere model.[8] The fundamental assumption of the DSMC method is that the particle movement and collision phases can be decoupled over time periods that are smaller than the mean collision time.

Recently, we expanded the DSMC method to simulate homogeneous condensation in the free expansions of argon,[9] a Lennard-Jones system, and the small polar molecules of water[10] and ethanol.[11] The studies showed that the cluster number density and size distributions are most sensitive to the nucleation model. Use of a *kinetic* versus a CNT rate for argon showed that the cluster sizes are about a factor of 20 smaller than for those obtained with CNT and the cluster number density is three to four orders of magnitude larger than for CNT.[12] For modeling water condensation in a large space-based plume,[13] we used CNT, but found the modeling results to be sensitive to the experimentally based CNT correction factor of Wolk *et al.*[14] They found that the CNT water nucleation rate in the temperature range from 220 to 260 K has to be corrected to match experimental data and the correction, a function of the water vapor temperature, can be large. For temperatures below 220 K, no correction to the rate is currently available.

In CNT, the nucleation process is modeled using the properties of the bulk fluid, such as, its density and surface tension. For supersonic expansions of Lennard-Jonesian systems and small polyatomic molecules, the critical cluster size can be as small as tens of monomers and one may expect that the bulk treatment of the process, such as the calculation of surface tension, is not appropriate.[15,16] In fact, for the specific flow conditions to be considered in this work, the main clusters in the flow are dimers and the use of CNT model would give an unreasonably high nucleation rate since the supersaturation ratio is so high that the critical cluster size is less than one. Therefore, because the nucleation rate drives the simulation results, the techniques developed in Ref. 12 to obtain a kinetic nucleation rate for argon must be expanded to enable the corresponding development for water.

To obtain accurate homogeneous condensation models, including nucleation, for small, polar molecules, such as water, accurate microscopic models suitable for implementation in DSMC need to be developed. Our previous work[10] employed a molecular dynamics (MD) method with the simple point charge (SPC) water potential to develop condensation models of water cluster-monomer collision and sticking probabilities to be used in DSMC simulations. Cluster size and cluster-monomer collision and sticking probability calculations were performed to verify that for the temperature and velocity ranges in a typical free expanding plume, the water clusters may be modeled with the HS collision model. The water sticking probabilities were found to decrease with cluster temperature and were shown to be significantly higher than the argon cases because the water dimer potential well depth is about 20 times larger than that of argon. The sticking probabilities were also found to increase with cluster size, as was observed in the work of Schenter *et al.*[15] and our values were similar to Ref. 15 especially for clusters larger than 10 mers. The MD simulation results were integrated into DSMC simulations of free expanding plumes studied experimentally in Ref. 5. Good agreement between the simulations and experiments were obtained if the classical nucleation rate was arbitrarily increased by a factor of 50.[10]

In order to develop a kinetic water nucleation model, the microscopic dimerization mechanism must be known. However, we are unaware of any experimental or even theoretical result that directly measures or simulates the kinetics of small water cluster formation. It is currently considered plausible (see Ref. 4) that dimers form by two competing channels: (1) bimolecular reactions involving metastable dimers and (2) termolecular collisions among water molecules.

Based on those two dimer formation rates, Crifo and Slanina[17] calculated the dimer mole fraction in a cometary

atmosphere, assuming a dimer formation rate as bimolecular and then termolecular. The formation rate is proportional to gas number density for bimolecular formation and to square of the gas number density for termolecular formation. In order to match CNT results, Crifo and Slanina used a dimer formation efficiency of 10^{-9} for bimolecular formations and 5×10^{-2} for termolecular formation. However, experimental or theoretical determinations of the dimer formation efficiency were missing. Moreover, in expanding plumes the gas number density drops so quickly that termolecular collisions are unlikely, which suggests that dimers are formed by bimolecular collisions.

Another study crucial to the research here is the work of Calo[18] in which his experimental studies of dimer formation in supersonic water vapor molecular beams are discussed. Assuming a termolecular dimer formation and bimolecular destruction kinetic model, he found that theoretical calculation results of dimer mole fractions as a function of source pressure, temperature, and orifice diameters agreed well with experiments.

The purpose of this work is to perform MD simulations to obtain the fundamental microscopic dimerization mechanism for the initiation of condensation in expanding water plumes. The model is then integrated into DSMC simulations of water vapor condensation. The simulations of several cases from the work of Calo[18] are discussed and compared. The paper is organized as follows. In Sec. II, MD simulations of supersaturated water vapor in a box, as well as in a free expansion, are introduced and the microscopic dimerization mechanism is studied. The bimolecular dimer formation probability is then calculated. Section III describes the integration of the bimolecular dimer formation model in the DSMC method. Section IV discusses the DSMC numerical parameters and procedures and the simulation results.

II. STUDY OF MICROSCOPIC MECHANISMS OF WATER DIMERIZATION

Hagena and co-worker[4,19] and Crifo and Slanina[17] postulated that dimers form primarily by two competing channels of bimolecular reactions involving metastable dimers or termolecular collisions among water molecules. In the bimolecular formation mechanism, two water molecules (M and M) collide and form a metastable dimer (orbiting pair, M_2) by the mechanism,

$$M + M \rightarrow M_2. \tag{1}$$

In a trimolecular formation mechanism, the two colliding molecules first form a collision complex M_2^*,

$$M + M \rightarrow M_2^*. \tag{2}$$

If the complex collides with a third molecule within its lifetime, it can then form a stable dimer M_2',

$$M + M_2^* \rightarrow M + M_2'. \tag{3}$$

To ascertain which of the above dimer nucleation mechanisms is important for the flow conditions in a supersonic expansion to vacuum, we performed MD simulations of a one-dimensional unsteady expansion. The MD simulations are analyzed to determine where and when a dimer is formed. In previous modeling of argon nucleation in a supersonic expansion,[12] the Stillinger geometric criterion was used to backtrack the origins of the cluster's formation. However, in this case, due to the complexity of the potential energy between two water molecules, a geometric criterion would be difficult to implement. In fact, the potential energy between two water molecules depends not only on the distance of the two oxygen atoms but also the orientation of the two molecules, especially for short oxygen-oxygen distances. Therefore, we first discuss the MD simulations of homogeneous nucleation in a box that enabled us to develop an efficient method to determine the existence of clusters (dimers) based on an energy criterion. By opening the box, we apply this algorithm to MD simulations of an expanding flow to locate dimers and obtain the collision history prior to their formation. We compare the temperature, number density, and Mach numbers obtained from the MD supersonic expansion with isentropic theory and discuss the relative importance of bimolecular versus termolecular dimer formation.

A. MD simulation of homogeneous nucleation in a box

Homogeneous nucleation of water was simulated using the MD LAMMPS code[20] for a cubic box system of size of $140\times140\times56$ Å with periodic boundary conditions in all directions. The number of molecules was 250 and the SPC (Ref. 21) potential model with a cutoff distance of 20 Å was the intermolecular potential used to model the interactions of water molecules. For the conditions in an expanding condensation flow, the water molecule temperatures are low compared to the characteristic vibrational temperatures so that it can be assumed that the vibrational energy is not activated. We therefore constrain the water molecules to be rigid with no energy transfer from translational to vibrational modes using the SHAKE (Ref. 22) algorithm to maintain rigid intramolecular water bonds. In the box simulations, the system density was chosen to be 6.80 kg/m^3 with a pressure corresponding to 5.27 atm, the plenum conditions of a case that we will consider with DSMC. The system was initially equilibrated at 1000 K for 50 ps and rescaled to 350 K, a temperature sufficiently low for condensation to occur, by simple velocity scaling[16] (the velocities of all the atoms in the system are scaled based on the square root of the temperature ratio). The system was run 1250 ps with a time step of 1 fs and a constant temperature of 350 K was maintained by simple velocity scaling. The density of saturated water vapor at $T=350$ K was found to be 0.466 kg/m^3 and the supersaturation ratio, S, was estimated to be about 14.6.

During the simulation at 350 K, the molecular position coordinates were exported every 1 ps. In order to determine the presence of clusters, we adopted the following energy criterion:[16] two molecules are defined to be connected (hydrogen bonded) if the potential energy between them is less than -10 kJ/mol where the SPC dimer potential well depth is -27 kJ/mol. We considered all pair interactions to determine all possible pairs of molecules with sufficient attraction between them to be considered bonded. For each output step,

we tabulated the number of bonds and neighbor molecules of each of the 250 molecules. Typically, per time step we accumulated a sample size of 1250 bonds. For each bond, the molecular ID was identified as well as the number of bonds the molecule had with the other 249 molecules and their corresponding molecular IDs.

In order to determine whether −10 kJ/mol is an accurate criterion, similar tables of bonds were made with different energy criteria. A comparison of the number of bonds at two different time steps of 100 and 200 ps for the energy criteria of −11, −10 and −9 kJ/mol showed no differences. Therefore, −10 kJ/mol is considered an appropriate energy criterion for determination of the connection of two molecules. Based on the bond tabulations, we can determine the number of dimers at different time steps. For example, if molecule 1 has only one neighbor, molecule 2, and molecule 2 also has only one neighbor, molecule 1, we say that molecule 1 and 2 exist as a single dimer. Once we locate a dimer, we trace back how it was formed. An example of a dimer formation process observed in the simulation was: water molecules 238 and 248 become bonded to form a dimer at 185 ps, although, they were not bonded at 184 ps. Since they continue to remain bonded from 186 to 200 ps, we consider them a stable dimer. In this simulation, we found ten dimers at 200 ps and all the ten dimers were formed from bimolecular collisions.

B. MD simulation of water dimerization in a one-dimensional expansion

Based on a similar method as introduced above, we performed MD simulations of a one-dimensional free expansion to determine the microscopic water dimerization mechanism for gas conditions closer to a nonequilibrium plume expansion. We use the MD technique to simulate not the entire supersonic free expanding plume system, which is computationally impossible, but rather a one-dimensional expansion similar to our previous argon condensation studies.[12] Once the dimer nucleation mechanism is identified and the rate is obtained, they are used in the DSMC simulations of the complete supersonic expansion.

The initial system is a oblong box with dimensions of $70\times70\times3584$ Å with periodic boundary conditions in all directions. Similar to Sec. II A, the system has 4000 molecules, which corresponds to a plenum density of 6.80 kg/m^3 at a corresponding pressure of 5.27 atm and temperature at 350 K. The system was initially equilibrated at 1000 K for 50 ps and rescaled to state at 350 K by simple velocity scaling.[16] The upper and lower periodic boundaries were then replaced with free boundary conditions to initiate a one-dimensional expansion. The simulation was then carried out for an additional 400 ps requiring 1 h of computational time of a 2.6 GHz processor. Figure 1 shows snapshots of the expansion at different time steps. During the simulation, the gas becomes rarefied as it expands over approximately four diameters in the axial direction and, at each time step, the number of molecules decreases with distance from the orifice, located at $z=0$.

The qualitative features of the one-dimensional expansion may be seen in Fig. 2 which presents the axial velocity component of the expanding water molecules at a time 200 ps after the opening of the orifice. The flow velocity at each axial location can be estimated by averaging the axial velocities of the molecules located at that distance, and the translational temperature is characterized by the corresponding velocity scatter. By analyzing the figure, one can see that the flow velocity (mean value of the velocities) increases and temperature (variance of the velocities) decreases with the distance, consistent with a one-dimensional isentropic expansion.

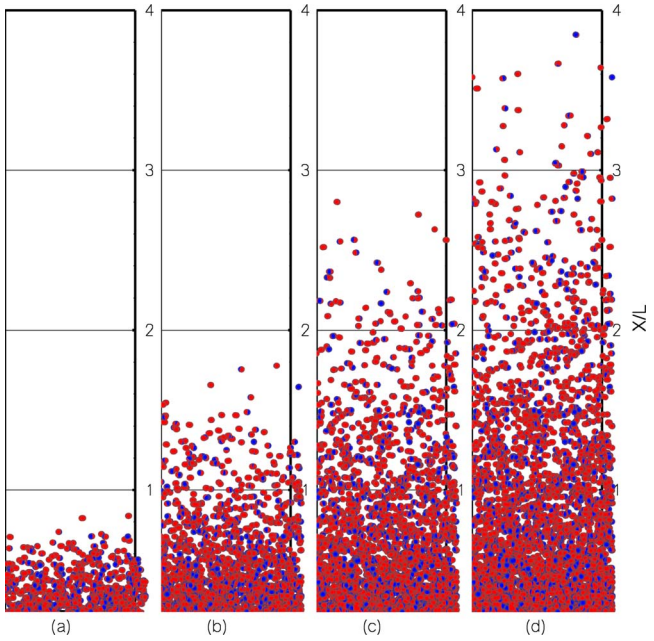

FIG. 1. (Color online) MD simulation of homogeneous nucleation in an expanding plume: molecular configurations at (a) 100, (b) 200, (c) 300, and (d) 400 ps. The origin of the *X* axial position is the orifice. The width of the orifice is *L*.

In addition to monomer and cluster velocities, the MD simulation data provides additional insight into the physics of the condensate, expanding flow. Figure 3 presents the number density, temperature, and Mach number obtained from the MD simulations within the entire computational domain at a time of 200 ps, i.e., after the upper transversal boundary is removed. The flow velocity and temperature at each axial distance are determined by the method discussed

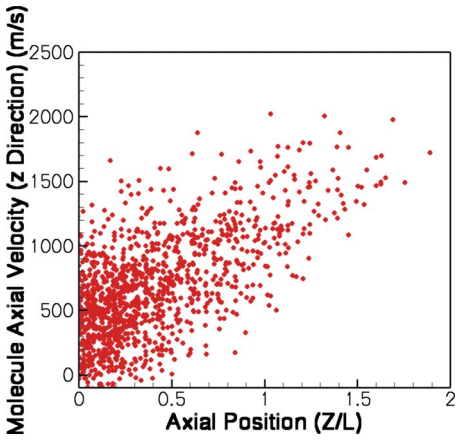

FIG. 2. (Color online) Axial velocity vs axial position of plume molecules at the end of MD simulation (200 ps).

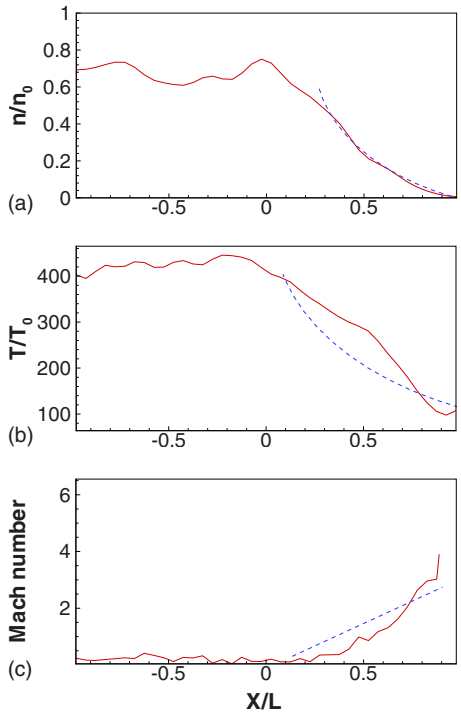

FIG. 3. (Color online) Number density (upper), translational temperature (middle), and Mach number (lower) as a function of axial location at a time of 200 ps (T_0=350 K and P_0=5.27 atm). Here, n_0 is the original number density. Solid lines are for simulation results and dashed lines for analytical results. Negative positions are inside the reservoir and positive positions are outside the reservoir.

above. The slight increase in the temperature inside the reservoir can be attributed to the release of latent heat during the condensation from the supersaturated reservoir gas. During the 200 ps simulation time, the gas expands to about 2 diameters in the axial direction. It can be seen that both the number density and temperature decrease outside the orifice and Mach number increase during the expansion. Also shown in Fig. 3 are the analytic solutions for number density, temperature, and Mach number based on one-dimensional isentropic expansion theory.[4] The comparison between isentropic theory and the MD results suggests that the MD simulation captures the essential physics of an expanding supersonic flow to vacuum. However, the higher temperature in the MD results demonstrates that the condensation is sufficiently strong that the condensation heat, which is not modeled in isentropic theory, increases the flow temperature.

Since the emphasis is to study the dimer formation mechanism in expanding plumes, we need to distinguish in the MD simulation those dimers that were created in the plume from those that were created in the reservoir and then transported into the plume. Figure 4 shows that the fraction of molecules belonging to clusters in the plume, estimated using the energy criterion to identify clusters, increases with time. However, during the same period of time, the fraction of molecules belonging to clusters in the reservoir also increases. Since the shapes of the curves shown in Fig. 4 are different, we can expect that at least part of the plume clusters have been formed in the plume. Using the same approach discussed in the previous subsection, we trace back how the dimers were formed. In the MD simulation, we

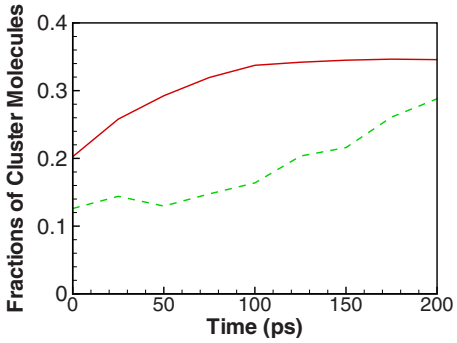

FIG. 4. (Color online) Time dependence of fractions of molecules that belong to clusters. Here solid line is for the fraction in the whole domain and dashed line for fraction in the reservoir.

found eight dimers and all of them were formed in the expanding flow downstream of the orifice through bimolecular collisions.

C. Relative contributions of dimer formation by binary and tertiary mechanisms in an expanding flow

From the MD expansion simulations, we found that dimers are created by bimolecular formation, rather than by a tertiary mechanism. Using simple kinetic theory arguments we deduce the ratio of dimer formation probabilities by the two mechanisms and confirm the MD results. Our starting point in the analyses is the sticking probability for a monomer-monomer collision [Eq. (1)]. In Sec. II D the manner in which we calculated this probability is discussed and it is shown that a typical probability of monomer-monomer sticking collisions is 0.035 for the temperatures and number densities occurring in a plume. From this value, we estimate the average nonsticking probability of a monomer-monomer collision, or the probability of creating a collision complex [Eq. (2)] is then $P_{\mathrm{cmlx}}=1-0.035=0.965$. Based on MD simulations for conditions where a large sample size of collision complexes can be created, the typical lifetime of a water collision complex is estimated to be $\tau=2.9$ ps. The collision frequency between a monomer, M, and a collision complex, M_2^*, is given by

$$\nu = \pi d^2 n g, \tag{4}$$

where ν is the collision frequency, d is the molecular diameter, n is the number density, and g is the average relative velocity. We consider a set of conditions picked from the free expansion MD simulation discussed above where the gas density is 0.68 kg/m^3, one-tenth of the plenum condition, the pressure is equal to 0.219 atm, and a temperature of 190 K. Since the average molecular thermal speed $\bar{v}$ is about 534 m/s, one obtains a collision frequency of $\nu=1.2840\times10^{10}$/s. The probability of collision between a complex and a monomer is then $\tau\times\nu=0.037$.

Based on similar MD simulations, the probability of creating a stable dimer from a collision between a monomer and a collision complex is 0.15. In summary, when a collision between two water molecules occurs, the probability of creating a stable dimer from a termolecular collision [Eqs. (2) and (3)] is $0.965\times0.037\times0.15=0.026$ compared to the

probability of metastable dimer formation via a bimolecular collision of 0.035. Although these probabilities are comparable, the typical density in an expanding flow drops rapidly favoring the bimolecular process that is proportional to the square of number density, n^2, rather than n^3 from a termolecular collision. In the latter case, the collision frequency between a dimer complex and a water molecule is even lower than for the bimolecular process, which further decreases the probability of creating a stable dimer by termolecular collisions. For this reason, we will use here the bimolecular dimer cluster formation mechanism instead of the termolecular mechanism.

Unlike the mono- or diatomic gases that Hagena studied,[19] a water dimer has more internal degrees of freedom that can absorb the released condensation heat when the two monomers collide and stick together. Moreover, the temperature of the monomers in the expanding plume considered here is sufficiently low such that the dissociation rate of the metastable dimers is low. For these conditions the water metastable dimers have a long lifetime and do not dissociate during the expanding process to the terminal steady-state plume where measurements of dimer mole fraction were made. In the later sections of this paper, we will denote the metastable dimers as simply dimers.

D. Monomer-monomer sticking probability

For the bimolecular formation mechanism, the sticking probability of monomer-monomer collisions is the dimer nucleation or formation probability, Eq. (1), and it is a function of the impact parameter, b, and total collision energy, E_c, or relative velocity, g. To determine the values of the sticking probability that will be used in the DSMC calculations to be discussed in Sec. III, inelastic monomer-monomer collisions were simulated with the MD method for various impact parameters and relative velocities, in a manner similar to our previous work.[10]

To utilize the MD results in the DSMC simulations, one needs to relate the physical conditions of the MD box simulations with those of a DSMC cell. The MD calculations are performed by equilibrating a system to a specified temperature. In DSMC, however, the equivalent system is a cell of typically 10–100 computational particles, each representing a large number of true, physical particles. The system of particles in the cell does usually does not have an equilibrium velocity distribution. In a DSMC time step (typically on the order of 0.01–1 μs), pairs of computational particles in a cell are picked at random and are then selected to be representative of a true binary collision based on the relative velocity, g.

For each relative velocity, g, the corresponding collision energy in a MD equipartition gas environment can be calculated by assuming that g is the average relative velocity, or

$$g = \sqrt{2}\bar{v}, \tag{5}$$

where $\bar{v}$ is the average molecular speed of a water monomer. By the equipartition principle, the corresponding average molecular rotational energy is $\bar{E}_r = \frac{1}{2}m\bar{v}^2$. If we neglect the monomer vibrational energy, the average total collision energy in an equipartition gas is given as

$$\bar{E}_c = \tfrac{1}{2}m_r g^2 + 2\bar{E}_r = \tfrac{3}{2}m\bar{v}^2 = \tfrac{3}{4}mg^2, \tag{6}$$

where $m_r = \frac{1}{2}m$ is the reduced mass, m is the water molecular mass, E_c is the collision energy, and E_r is the rotational energy. Using the last equality of Eq. (6) we have a one-to-one correspondence between g and $\bar{E}_c$. For any total collision energy E_c in our DSMC calculation, we can therefore calculate g and the corresponding MD sticking probability.

The sticking probability for each MD simulation case (b, g) is defined as the ratio of the number of trajectories that resulted in a sticking collision to the total number of trajectories. The target water molecule is placed at the origin with a center-of-mass velocity of zero and with an internal rotational energy of $\frac{1}{4}mg^2$. The collider molecule with the same internal rotational energy as the target molecule is initially separated 20 Å from the target molecule such that the interaction potential between them is effectively zero. For each case, a sample of 2500 trajectories is obtained with an orientation of the target monomer and collider monomer randomly chosen. The total simulation time for each case is approximately 50 ps, which is long enough to observe whether the interaction outcome is a sticking or nonsticking event since it takes about 5 ps before the collider travels into the vicinity of the target monomer. The impact parameter b increases from a head-on collision value of zero to a maximum value for which the monomer-monomer collision probability is close to zero. Collision relative velocities from approximately 305 to 933 m/s are chosen, corresponding to a typical plume gas temperature of 40–370 K.

In a DSMC simulation of an expanding flow, consisting of gas and cluster species, each collision is not modeled in detail and only average collision properties are used. For this reason, the dependence of the sticking probability must be averaged over impact parameter. The average sticking probability, P^i_{av}, can be calculated from the MD results for each cluster based on a b^2 distribution of collision pairs,

$$P^i_{\mathrm{av}} = \frac{1}{b^2_{i,m}}\int_0^{b_{i,m}} P(b)db^2, \tag{7}$$

where $b_{i,m}$ is the cluster maximum impact parameter or collision radius for a cluster of size i.

Figure 5 shows that the monomer-monomer sticking probability (solid line) decreases as the relative velocity increases and for velocities greater than 700 m/s, the probability is almost zero. Also shown are the dimer-monomer sticking probabilities (dashed line) obtained in our previous work.[10] The monomer-monomer sticking probabilities are always lower than those of dimer-monomers since the dimer-monomer potential well depth is much higher. In Sec. III we explain how the monomer-monomer sticking probabilities shown in Fig. 5 are used to create a DSMC nucleation model.

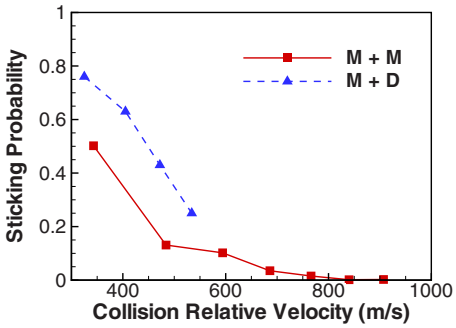

FIG. 5. (Color online) Water monomer-monomer sticking probability (solid line) for collision velocity from 305 to 933 m/s. Also shown are water dimer-monomer sticking probabilities from Ref. 10 (dashed line).

III. IMPLEMENTATION OF THE BIMOLECULAR DIMER FORMATION MODEL IN DSMC

In DSMC simulations, the flow field is created from multiple collision events that replicate the local kinetic collision frequency. In SMILE,[23] the DSMC computational tool used in this work, the collisional algorithm is based on the majorant frequency scheme.[24] The general idea behind the algorithm is to efficiently pick collision pairs of computational particles in a random manner. The probability of a collision occurring for that pair is evaluated based on the pair's relative velocity and collision cross section. If the probability passes an acceptance-rejection test, the pair is accepted as representing a binary collision. The type of collision still needs to be assessed. Collisions are classified into the following three groups: both colliding particles are dimers, one of the particles is an dimer, or both particles are monomers.

In the last case, the outcome of the collision, dimer formation, is possible and is assumed to proceed via the mechanism given in Eq. (1). To evaluate the outcome of the sticking probability event (the sticking probability), the total collision energy of the selected pair, E_c, must be determined. The total energy of the colliding pair, E_c, may be written as

$$E_c = E_t + E_{i1} + E_{i2}, \tag{8}$$

where E_t, is the relative translational energy and $E_{i,1,2}$ is the internal energy of molecule 1 or 2. Note that $E_{i,1,2}$ includes both the rotational ($E_{r,1,2}$) and vibrational energies ($E_{v,1,2}$) of molecule 1 or 2; however, since the plume condensation-flow gas temperatures are low, we assume that the internal vibrational energy contribution is zero. The relative translational energy is obtained from the DSMC velocity vector components for the pair of computational molecules as follows. The center-of-mass velocity, $\mathbf{V}$, and the relative velocity, g, are

$$\mathbf{V} = \tfrac{1}{2}((\mathbf{v}_1 + \mathbf{v}_2)\ , \tag{9}$$

$$\mathbf{g} = \mathbf{v}_1 - \mathbf{v}_2, \tag{10}$$

where $\mathbf{v}_1$ and $\mathbf{v}_2$ are the presticking translational velocities of water computational molecules 1 and 2. Since the total translational kinetic energy is given as

$$\mathbf{TE} = \tfrac{1}{2}mv_1^2 + \tfrac{1}{2}mv_2^2 = m\mathbf{V}^2 + \tfrac{1}{4}mg^2 = m\mathbf{V}^2 + E_t, \tag{11}$$

we have

$$E_t = \tfrac{1}{4}mg^2, \tag{12}$$

which, when used in Eq. (8) above, permits the evaluation of the total collision energy of the pair.

Based on the total collision energy, the outcome of the collision is determined based on the acceptance-rejection test using the sticking probabilities computed by the MD calculations discussed earlier in Sec. II D. If a dimer is formed, its velocity is $\mathbf{V}$ and the internal energy after the collision is given as

$$E_i' = E_c + Q, \tag{13}$$

where Q is the latent heat released by the dimerization process and here we use a constant value of -8.8 kcal/mol taken from Ref. 15. The dimer internal energy is then distributed among its rotational and vibrational modes by use of the equipartition principle. The number of rotational degrees of freedom of a cluster is 3 and the number of vibration degrees of freedom can be calculated as $6N-3-3=6$, where N is the number of water molecules inside a cluster and there are three translation and three rotational degrees of freedom for a water cluster. Here we used constraint dynamics[25] but assumed that bonds between molecules inside a cluster are too weak to be considered as constraints.

In addition, when a collision occurs between a cluster (e.g., a dimer) and a monomer, it can result in either a sticking or nonsticking process based on the sticking coefficient probability, also precalculated from MD simulations.[10] Nonsticking collisions are treated in the same way as monomer-monomer nonsticking collisions and are modeled by the VHS model.[8] A sticking collision between a cluster and a monomer is referred to as condensation. When a condensation event occurs, the monomer effectively becomes a part of the cluster. In an evaporation process,

$$\mathrm{M}_{i+1} \rightarrow \mathrm{M}_i + \mathrm{M} \tag{14}$$

monomers are removed from a cluster and it is assumed that each evaporation event involves the removal of one monomer from a cluster at a time. When an evaporation event occurs in the DSMC simulation, the cluster size is reduced by one, and one new monomer is randomly created in the computational cell. Finally, when two clusters collide with each other, it can also result in either a nonsticking (modeled by VHS model) or sticking process. However, since the cluster density is so low in this work, we do not model cluster-cluster sticking collisions. Detailed description of these models and their specific implementation in DSMC can be found in Ref. 26.

IV. RESULTS AND DISCUSSIONS

The kinetic condensation models discussed above, including the new, bimolecular nucleation model are applied to the free expansion of an orifice condensation beam experimentally studied by Calo.[18] An orifice with a diameter of 125 μm is attached to a chamber with stagnation pressures, P_0, of 40–120 torr and stagnation temperatures, T_0, of 373–493 K. The water vapor inside the chamber expands through the orifice into a vacuum environment and condensation oc-

curs outside the chamber. The influence of the stagnation temperature and orifice diameter on the dimer mole fraction was investigated and discussed in Ref. 18.

The DSMC simulation under consideration is challenging due to the large variation in number density from the chamber to the plume far field. The Knudsen number, defined as the ratio of mean free path to the characteristic length (the orifice diameter), is on the order of 10^{-3} at the orifice. This low Knudsen number indicates that a DSMC computation cell length of 10^{-6} m is required and, based on the speed of the flow (500 m/s at the orifice), a time step on the order of 10^{-8} s is necessary. Since the flow is expanding, however, such small cell sizes and time steps is not necessary for most of the computational domain and would be impractical.

The DSMC computational cost is reduced by the use of two successive DSMC calculations, a valid numerical approach since the flow is supersonic. The first calculation (designated as "near field") is started inside the chamber and carried out to a small region beyond the orifice. The reservoir is located on the left side of the wall shown as the left boundary of the computational domain in Fig. 6. The gas expands through the orifice, which is located in the low-left corner, along the X axis and the flow is axisymmetric. The near-field region is the small white region close to the nozzle orifice seen in Fig. 6 and subsequent figures. The converged near-field DSMC macroparameters of gas temperatures, velocities, and number densities are then used to create a starting surface for the second DSMC, "far field" calculation. The starting surface is located just down stream of the orifice. The computational parameters for the near and far-field calculations are given in Table I. In this paper we emphasize the far-field results and additional details may also be found in Ref. 23. To obtain the steady-state cluster characteristics, such as terminal cluster mole fraction, a computational domain of 10 orifice diameters in both axial and radial directions was utilized. A species weighting factor of 10^{-2} for water dimers was used to improve the resolution of dimer species. A typical simulation requires about 5 h of computational time with 32 3.06 GHz processors. Two types of DSMC studies were performed. First the stagnation pressure was held constant and five stagnation temperature cases were considered. Then the stagnation temperature was held constant and the stagnation pressure was varied.

The general features of the DSMC supersonic flow to vacuum may be seen in Fig. 6. The upper and middle figures show the gaseous water number density and translational temperature contours, respectively, of the condensation plume for the case T_0=438 K and P_0=100 torr. As the water vapor undergoes free expansion, the number density drops by three orders of magnitude and the temperature decreases rapidly from 340 to 20 K. In these figures, as well as subsequent ones, the orifice is located at the origin.

It can be seen in Fig. 6 that the initial dimers appear in a nucleation region (left corner where the starting surface is located), the location where the cluster number density increases quickly along the flow direction. Downstream of the nucleation region, the cluster number density decreases, mainly due to the expansion. Since the dimer number density

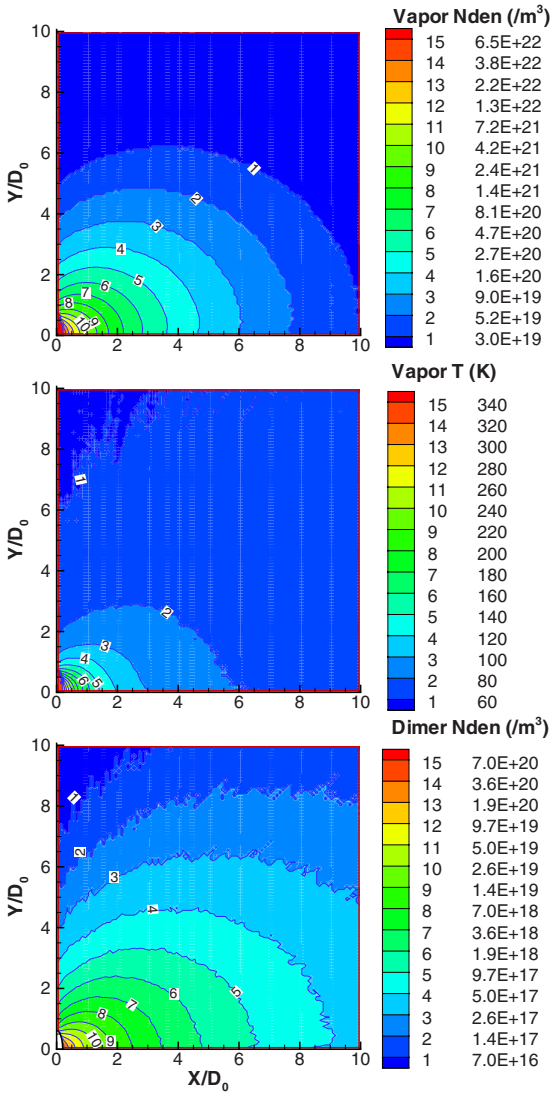

FIG. 6. (Color online) Gaseous number density (upper), gaseous temperature (middle), and dimer number density (lower) contours in the condensation plume (T_0=438 K, P_0=100 torr). Here X is the axial direction, Y is the radial direction, and D_0 is the orifice diameter.

is only on the order of $10^{19}/\mathrm{m}^3$, the condensation process does not affect the gaseous flow. Due to the latent heat and nonequilibrium, the dimer temperature is higher than the surrounding water vapor molecules as shown along the plume centerline in Fig. 7.

To provide a quantitative comparison of the condensate flow for the five different stagnation temperature cases, number density, translational temperatures, and dimer mole fractions along the plume center line are shown in Fig. 8. The dimer mole fractions is the ratio of the dimer cluster to gas

TABLE I. Computational parameters in the DSMC simulations.

Calculations	Near-field	Far-field
Time step (s)	2×10^{-8}	1×10^{-8}
F_{num}	2×10^{7}	5×10^{5}
Domain size (m^2)	0.0012×0.006	0.001×0.001
Numerical cells	240×120	100×100
Numerical computational particles	6.6×10^{4}	3.5×10^{4}

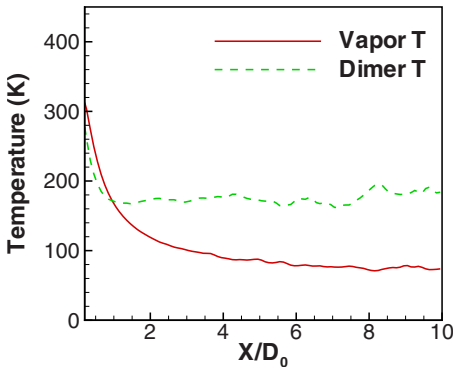

FIG. 7. (Color online) Gaseous and dimer translational temperatures along the plume centerline (T_0=438 K, P_0=100 torr).

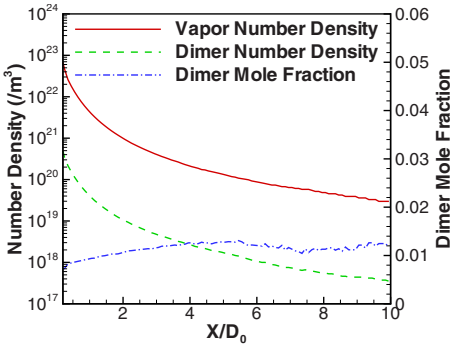

FIG. 9. (Color online) Water vapor number density, cluster number density, and dimer mole fraction along the plume centerline (T_0=438 K, P_0=100 torr).

and cluster number densities. The large majority of the cluster is found to be dimers, with only about 4%–5% of the clusters being trimers. It can be seen in Fig. 8 that the normalized number density drops three orders of magnitude for all cases with similar spatial dependence and with cases T_0 =373 and 493 K dropping slowest and fastest, respectively. The higher the stagnation temperature, the stronger the gas expansion and the faster the density drop. The translational temperatures decrease quickly for all the cases due to the expansion, as shown in Fig. 8 and remains constant beyond $X=2D_0$. The dimer mole fraction profiles shown in Fig. 8 increase upstream of $X=2D_0$ due to the high number of bimolecular collisions, and increase slowly thereafter due to the plume expansion.

Water vapor, cluster number density, and dimer mole fraction along the plume centerline for T_0=438 K and P_0 =100 torr are shown in Fig. 9. It can be seen that the cluster number density is about two orders of magnitude less than the vapor number density and the average dimer mole fraction along the centerline is about 0.009. The dimer mole fraction quickly increases along the centerline and increases more slowly after $X=2D_0$ which indicates that there are few collisions. The dimer mole fraction value beyond $X=2D_0$ is the terminal mole fraction, a value which is typically reported in experiments.

The comparison between simulation and experiment is presented in Figs. 10 and 11. Figure 10 shows the comparison of the terminal water dimer mole fractions with the experimental data of Calo for different reservoir stagnation temperatures. It can be seen that our terminal mole fraction

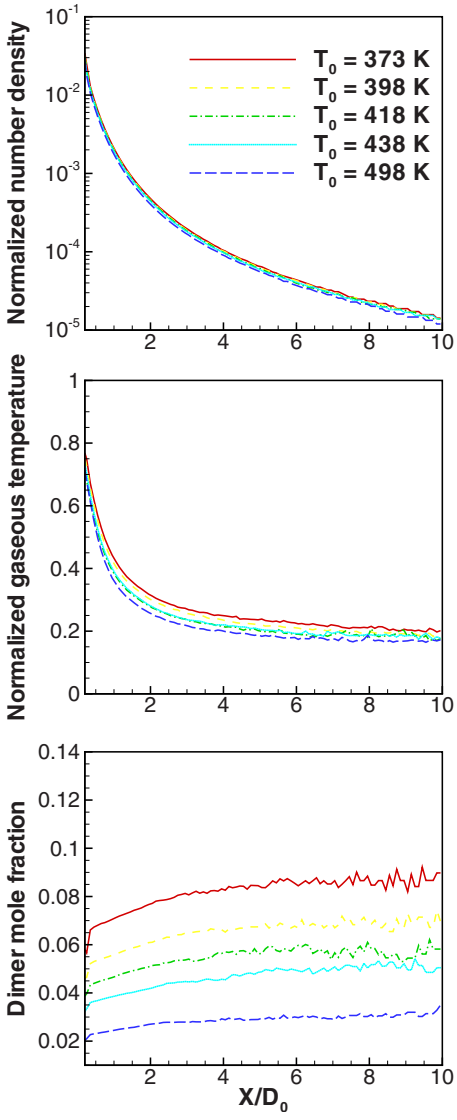

FIG. 8. (Color online) Number density (upper, normalized by stagnation number densities), gaseous temperature (middle, normalized by stagnation temperatures), and dimer mole fraction (lower) along the plume centerline for different stagnational temperatures (P_0=100 torr).

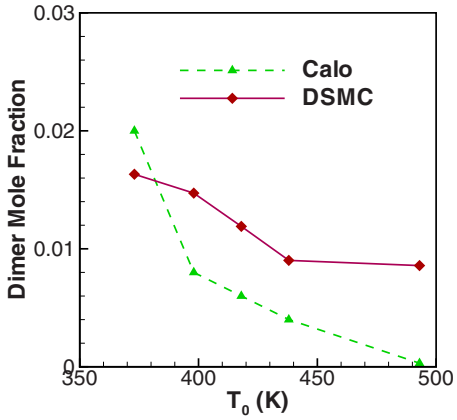

FIG. 10. (Color online) Comparison of terminal water dimer mole fractions with Calo's (Ref. 18) experimental data for different reservoir stagnation temperatures (P_0=100 torr).

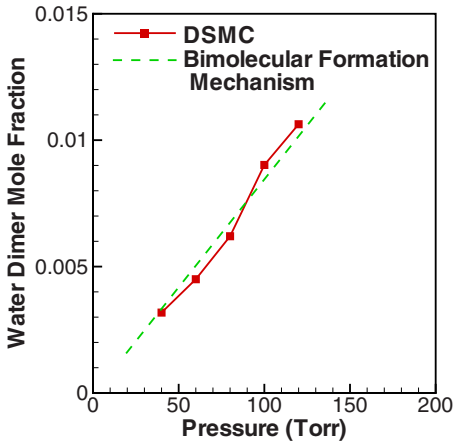

FIG. 11. (Color online) Terminal water dimer mole fractions for different reservoir stagnation pressures (T_0=438 K).

decreases as the reservoir stagnation temperature increases, which is similar to Calo's experimental results, and the values are close (differences are within a factor of 2). Figure 11 shows that the predicted terminal water mole fractions are proportional to the stagnation pressure in the range of 40–120 torr, at a constant stagnation temperature of 438 K. According to the classical nucleation theory, the nucleation rate is proportional to the square of vapor number density. Since the degree of condensation is low in all the cases considered, the condensation effect does not significantly change the vapor number density, i.e., the vapor number density is the same as in noncondensation cases. Furthermore, in noncondensation cases, vapor number density is proportional to the stagnation number density. The nucleation rate is therefore proportional to the square of chamber number density. Since the condensation and evaporation processes are not significant for these cases either, the dimer cluster density is proportional to the nucleation rate or to the square of chamber number density or stagnation pressure. The corresponding terminal dimer mole fraction should be proportional to the chamber stagnation pressure. This linear pressure-dependent result is constant with both the bimolecular formation mechanism and Calo's theoretical prediction.

V. CONCLUSIONS

In this work, we performed MD simulations of homogeneous condensation in a box and in a free expansion to explore the microscopic mechanism of water dimer formation and bimolecular formation was found to be the main mechanism. The relative contribution of bimolecular to trimolecular dimer formation was evaluated and found to be more important for the typical conditions in a free expansion. The probability of bimolecular dimer formation by collisions between two water molecules as a function of collision energy were obtained by MD simulations and it is observed that the probability decreases with collision energy.

The dimer formation probabilities and postcollisional velocity and energy distributions were then integrated into DSMC simulations of a free expansion through an orifice condensation plume with different chamber stagnation temperatures. The dimer mole fraction increases with distance from the orifice and becomes constant after a distance of about 2 orifice diameters. The terminal dimer mole fraction was found to decrease with chamber stagnation temperatures similar to the experiment. Simulations also suggest that the mole fraction increases linearly with chamber stagnation pressures which is consistent with simple kinetic theory for a bimolecular nucleation mechanism.

ACKNOWLEDGMENTS

The research performed at the Pennsylvania State University was supported by the Air Force Office of Scientific Research under Grant No. F49620-02-1-0104 and the Chemistry Division of the National Science Foundation under Grant No. CHE-0456514 whose supports are gratefully acknowledged. Special thanks are to Professor M. Ivanov of the Institute of Theoretical and Applied Mechanics, Russia for the use of the original SMILE code and Dr. G. K. Schenter for helpful discussions.

[1] C. E. Kolb, R. B. Lyons, J. B. Elgin, R. E. Huffman, D. E. Paulsen, and A. McIntyre, J. Spacecr. Rockets **20**, 383 (1983).
[2] M. S. Ivanov and G. N. Markelov, J. Propul. Power **15**, 417 (1999).
[3] B. J. C. Wu, AIAA J. **13**, 797 (1975).
[4] O. F. Hagena and W. Obert, J. Chem. Phys. **56**, 1793 (1972).
[5] W. D. Williams and J. W. L. Lewis, "Summary report for the CONSET program at AEDC," DTIC Paper No.. AEDC-TR-80-16, September 1980, http://www.dtic.mil/dtic.
[6] G. Koppenwallner and C. Dankert, J. Phys. Chem. **91**, 2482 (1987).
[7] A. Ramos, J. M. Fernández, G. Tejeda, and S. Montero, Phys. Rev. A **72**, 053204 (2005).
[8] G. A. Bird, *Molecular Gas Dynamics and the Direct Simulation of Gas Flows* (Clarendon, Oxford, 1994).
[9] J. Zhong, M. I. Zeifman, and D. A. Levin, J. Thermophys. Heat Transfer **20**, 41 (2006).
[10] Z. Li, J. Zhong, D. A. Levin, and B. Garrison, AIAA J. **47**, 1241 (2009).
[11] A. C. Gallagher-Rogers, J. Zhong, and D. A. Levin, J. Thermophys. Heat Transfer **22**, 695 (2008).
[12] J. Zhong and D. A. Levin, AIAA J. **45**, 902 (2007).
[13] J. Zhong, M. I. Zeifman, and D. A. Levin, J. Thermophys. Heat Transfer **20**, 517 (2006).
[14] J. Wolk, R. Strey, C. H. Heath, and B. E. Wyslouzil, J. Chem. Phys. **117**, 4954 (2002).
[15] G. K. Schenter, S. M. Kathmann, and B. C. Garrett, J. Chem. Phys. **116**, 4275 (2002).
[16] K. Yasuoka and M. Matsumoto, J. Chem. Phys. **109**, 8463 (1998).
[17] J. F. Crifo and Z. Slanina, Astrophys. J. **383**, 351 (1991).
[18] J. M. Calo, J. Chem. Phys. **62**, 4904 (1975).
[19] O. F. Hagena, in Proceedings of the 6th International Symposium on Rarefied Gas Dynamics, edited by L. Trilling and H. Y. Wachman (Academic, New York, 1969), pp. 1465–1468.
[20] S. J. Plimpton, J. Chem. Phys. **117**, 1 (1995).
[21] H. J. C. Berendsen, J. P. M. Postma, W. F. van Gunsteren, and J. Hermans, in *Intermolecular Forces*, edited by B. Pullman (Reidel, Dordrecht, 1981), pp. 331–342.
[22] J. P. Ryckaert, G. Ciccotti, and H. J. C. Berendsen, J. Comput. Phys. **23**, 327 (1977).
[23] M. S. Ivanov, A. V. Kashkovsky, S. F. Gimelshein, G. N. Markelov, A. A. Alexeenko, Ye. A. Bondar, G. A. Zhukova, S. B. Nikiforov, and P. V. Vashenkov, in "*SMILE System for 2D/3D DSMC Computations*," Proceedings of the 25th International Symposium on Rarefield Gas Dynamics, St. Petersburg, Russia, 21–28 July 2006, edited by M. S. Ivanov and A. K. Rebrov (Publishing House of the Siberian Branch of the Russian Academy of Sciences, Novosibirsk, 2007), pp. 539–544.
[24] M. S. Ivanov and S. V. Rogasinsky, Sov. J. Numer. Anal. Math. Modeling **3**, 453 (1988).
[25] D. T. Greenwood, *Principles of Dynamics* (Prentice-Hall, Englewood Cliffs, NJ, 1987).
[26] J. Zhong, Ph.D. thesis, The Pennsylvania State University, 2005.